Nano Energy 56 (2019) 92–99

Contents lists available at ScienceDirect

Nano Energy

journal homepage: www.elsevier.com/locate/nanoen

Full paper

A MOF-based single-ion Zn^{2+} solid electrolyte leading to dendrite-free rechargeable Zn batteries

Ziqi Wang, Jiangtao Hu, Lei Han, Zijian Wang, Hongbin Wang, Qinghe Zhao, Jiajie Liu, Feng Pan*

School of Advanced Materials, Peking University Shenzhen Graduate School, Shenzhen 518055, PR China

ARTICLE INFO

Keywords:
Solid-state electrolytes
Zn batteries
Single-ion conductors
Metal–organic frameworks
Post-synthetic modifications

ABSTRACT

Rechargeable Zn ion battery is a promising alternative for the current portable and mobile energy storage technologies because of its good safety, low cost, and material abundance. Poor deposition reversibility with dendrite formation of Zn metal anode in aqueous electrolytes, which brings the risk of short-circuit and capacity loss (dead Zn), is one of the critical issues that plague its practical applications. To improve the performances of Zn ion batteries, a crystalline single-ion Zn^{2+} solid-state electrolyte (SSE) is designed based on a post-synthetic modified metal–organic framework. The SSE possesses many advantages such as high ionic conductivity of 2.1×10^{-4} S cm^{-1} at 30 °C, minor activation energy of 0.12 eV, high Zn^{2+} transference number of 0.93, along with the good mechanical and electrochemical stability. Due to the restricted and guided Zn deposition through the nanowetted Zn/SSE interface at which $Zn(H_2O)_6^{2+}$ ions are confined, excellent compatibility between Zn metal anode and the SSE is revealed, which is confirmed firmly by the stable Zn plating/stripping performance, giving rise to a homogeneous, compact, and smooth Zn deposition layer. The good properties of the SSE are further verified in VS_2/Zn batteries, which deliver a reversible capacity of 125 mAh g^{-1} over 250 cycles at 0.2 A g^{-1} and a reasonable rate capability with ~40% capacity retention (vs. 0.1 A g^{-1}) at 2 A g^{-1}.

1. Introduction

Alternative rechargeable battery technologies are urgently needed due to the high-cost and safety concerns of the today used lithium ion batteries. Among the various candidates, aqueous Zn ion batteries (ZIBs) are considered to be the most attractive choice because Zn metal is naturally abundant and non-toxic, and aqueous electrolytes are much safer [1,2]. Meanwhile, Zn anode has a low redox potential (-0.76 v.s. the standard hydrogen electrode) and its volumetric capacity is nearly 3 times higher than that of Li due to the two-electron redox ($Zn^{0/2+}$) and high density (7.13 g cm^{-3}) [3]. The poor deposition reversibility and dendrite issue of Zn metal anode are great challenges that hinder the practical applications of ZIBs [2]. Although dendritic deposition of Zn can be alleviated in neutral electrolytes in some way [4], compact and homogenous deposition is still hard to realize. Instead, a porous layer assembled by randomly distributed Zn plates/protrusions usually forms [1,5]. Such loose and rough Zn deposition layer will pulverize during long-term cycling causing irreversible capacity loss (dead Zn) and even battery short circuit [6]. Many endeavors have been made recently to solve this issue. Wang and co-workers [2] found that the reversibility of Zn anode can be effectively improved by using the electrolyte containing highly concentrated $TFSI^-$ salts, but the use of $TFSI^-$ dramatically increases the material cost. Kang and co-workers [6] reported that homogenous Zn deposition without large protuberances can be achieved by coating a layer of porous $CaCO_3$ onto the surface of Zn anode, but some microsized Zn flakes still exist, in face of the pulverization risk during cycling. Until now, solutions to the reversible Zn metal anode are inadequate and urgently needed.

The deposition morphologies of Zn metal rely much on the electrolyte [2,7]. Solid-state electrolytes (SSEs), which have been used to prevent dendrite formation in Li batteries by virtue of the mechanical robustness, high Li^+ transference number ($t_{Li+} = 1$, theoretically) and capability of uniform Li deposition [8,9], would be a promising avenue to improve the applicability of Zn metal anode. Unfortunately, rare Zn SSEs have been reported so far because of the strong electrostatic bonding nature of the divalent Zn^{2+} ions which results in slow diffusion kinetics and low ionic conductivity [10].

Here, for the first time, we report a crystalline single-ion Zn^{2+} SSE based on a post-synthetic modified metal–organic framework (MOF) with fixed anionic microporous host and mobile Zn^{2+} ions. The electrical insulated MOFs with large cavities which enable fast ion movement are excellent platforms to design solid electrolytes for batteries [11,12]. The properties of MOFs can be tailored for different applications through post-synthetic modification [13], which has also been used to create ion conductive MOFs. By replacing the coordinated water

* Corresponding author.
E-mail address: panfeng@pkusz.edu.cn (F. Pan).

https://doi.org/10.1016/j.nanoen.2018.11.038
Received 13 September 2018; Received in revised form 25 October 2018; Accepted 14 November 2018
Available online 16 November 2018

in the second building units (SBUs) with LiOR, Long and co-workers [14] reported a UIO-67-based Li^+ SSE, but the relatively low ionic conductivity restricts its practical application in batteries. Dincă's group reported a series of single-ion conductors based on the post-synthetic modified MIT-20. These ionic conductors demonstrated high conductivity, but their electrochemical windows (EWs) are speculated to be limited by the redox-active Cu(II) centers in MOFs. Ideally, the MOF-based Zn^{2+} SSE should be both highly conductive and electrochemically stable upon battery operations.

MOF-808 [15] with robust $Zr_6(O)_4(OH)_4(HCO_2)_6$ SBUs is used here to design Zn solid electrolyte. The neutral MOF-808 becomes negatively charged with high charge density after HCl treatment, and the H^+ counter ions in its pores are then replaced with $Zn(H_2O)_6{}^{2+}$ to offer a novel single-ion Zn^{2+} SSE, which exhibits a high conductivity of 2.1×10^{-4} S cm^{-1} at 30 °C with small activation energy of 0.12 eV and high Zn^{2+} transference number of 0.93. It also demonstrates good compatibility with Zn metal anode and favored dendrite-free, smooth, and compact Zn deposition benefited from its solid microporous structure with nanowetted interface between SSE and Zn metal. Such nanowetted interface is created by the electrochemically driven desolvation of $Zn(H_2O)_6{}^{2+}$ confined within anionic MOF host at the Zn anode surface, which results in H_2O release leading to interfacial wetting and Zn^{2+} deposition with redox reaction indicated as $Zn^{2+} + 2e^- = Zn$. Note that the microporous structure with nanowetted interface plays the key role to restrict and guide uniform Zn deposition to avoid free-dendrite growth, in contrast to the normal unrestricted bulk-solution/Zn-metal interface. The VS_2|SSE|Zn solid batteries assembled deliver a stable cycling performance with a specific capacity of 125 mAh g^{-1} over 250 cycles at 0.2 A g^{-1}, and show a reasonable rate capability with about 40% capacity retention at 2 A g^{-1}.

2. Results and discussion

2.1. Post-synthetic modification and characterization

The post-synthetic modification chemistry is displayed in Fig. 1a. Uniform polyhedron MOF-808 ($[Zr_6O_4(OH)_4(HCOO)_6(BTC)_2]$) nanocrystals with a diameter of 100–150 nm were prepared by a solvothermal reaction [16] between $ZrOCl_2{\cdot}8H_2O$ and 1,3,5-benzenetricarboxylic acid (BTC), as characterized by scanning electron microscopy (SEM) in Fig. S1a. The phase purity was confirmed by the X-ray diffraction (XRD) pattern (Fig. S2) which is well consistent with the simulated result. Six formic acids are coordinated in each $Zr_6(O)_4(OH)_4(HCO_2)_6$ SBU of MOF-808 according to the reported structure [15], which can be proved by the ^{1}H nuclear magnetic resonance (NMR) in Fig. 1c. The neutral MOF-808 was turned negative (six negative charges per SBU) by removing these capping formate groups through HCl treatment [16] to afford HMOF-808 ($[Zr_6O_4(OH)_4(OH)_{12}H_6(BTC)_2]$), in which less than 8% of formate groups were remained judging from the ^{1}H NMR result. ZnMOF-808 ($[Zr_6O_4(OH)_4(OH)_{12}Zn_3(BTC)_2]$) was obtained by replacing the counter H^+ ions in HMOF-808 with Zn^{2+} ions. For better H^+ extraction, we used zinc acetate solution as medium in the cation exchange process in view of its relatively higher pH among the zinc salt solutions. The cation exchange was repeated until a high exchange rate of 91.2% (Fig. 1d) was achieved as determined by inductively coupled plasma (ICP) test, corresponding to 2.7 Zn per SBU. XRD (Fig. S2) and SEM (Fig. S1) of HMOF-808 and ZnMOF-808 indicates the MOF structure and morphology were almost unchanged after the post-synthetic modification due to the excellent chemical stability. Fig. S3 shows the N_2 adsorption/desorption isothermals of MOF-808 and ZnMOF-808 at 77 K. The Brunauer-Emmett-Teller (BET) surface area and pore volume of MOF-808 were calculated to be 1608 m^2 g^{-1} and 1.15 cm^3 g^{-1}, respectively, which dropped to 662 m^2 g^{-1} and 0.71 cm^3 g^{-1} for ZnMOF-808 as a result of Zn^{2+} uptake. For the purpose of normal battery assembly, the mechanical stability of ZnMOF-808 was tested under high pressure and then characterized by XRD. In Fig. S2, the ZnMOF-808 pellet (ϕ 12 mm) pressed under 10 t force shows identical reflection peaks with its powder form, indicating the porous crystal structure was intact after being compressed.

2.2. Single-ion Zn^{2+} conductivity

Initially, the activated ZnMOF-808 has a very low conductivity of 3×10^{-7} S cm^{-1} at room ambient indicating Zn^{2+} ions are tightly bonded to the MOF host. However, upon absorbing some water at higher humidity, Zn^{2+} ions in the pores of MOF become solvated and conductive, affording the water@ZnMOF-808 (WZM) SSE. Typically, about 30 wt% of H_2O guest is contained in the WZM SSE by exposing the activated ZnMOF-808 at 60 °C, 90% relative humidity (RH) for 24 h, according to the thermogravimetric analysis (TGA) test shown in Fig. S4. It should be noted that the WZM SSE still demonstrates a "free-flowing" dry powder appearance indicating complete water impregnation driven by the high porosity and high hydrophily of the ZnMOF-808 host. Because of the strong water-capturing ability of MOF host, water content in WZM SSE is relatively stable. As shown in Fig. S5, only 4 wt% water loss was observed when WZM SSE was exposed to room ambient for 1 h, and 91 wt% water guest could be maintained after 24 h. To determine the ionic conductivity, WZM SSE powder was pressed into pellet and sandwiched between two stainless steel (SS) electrodes to conduct electrochemical impedance spectroscopy (EIS) test. Water loss in WZM SSE during test can be prevented by tightly sealing the SS|WZM|SS cell with resin, which is confirmed by comparison of conductivity results for the cells heated at 80 °C for 20 h, as shown in Fig. S6. Arrhenius plot for the conductivities and corresponding EIS from 30° to 90°C of WZM SSE are shown in Fig. 2a and Fig. 2b. It demonstrates a high conductivity of 2.1×10^{-4} S cm^{-1} at 30 °C with small activation energy of 0.12 eV (Fig. S7), which is remarkable relative to the reported MOF-based electrolytes, as summarized in Tab. S1. Unlike ceramic Li SSEs such as $Li_7La_3Zr_2O_{12}$ (LLZO) and $Li_{1+x}Al_xTi_{2-x}(PO_4)_3$ (LATP), the Zn^{2+} ions in MOF crystals are solvated by water, and their conducting mechanism is similar to that of liquid electrolytes containing Zn^{2+} ions. On account of the shielding effect of the coordinated water shell, $Zn(H_2O)_6{}^{2+}$ ions show negligible bonding interaction with the MOF host, which then results in the high conductivity and small activation energy. The comparison of electrochemical windows (EWs) between WZM SSE and 1 M $ZnSO_4$ aqueous electrolyte was further studied by linear sweep voltammetry (LSV) tests at 0.2 mV s^{-1} on the coin cells using SS as working electrode and Zn metal as reference and counter electrodes. The oxygen evolution reaction (OER) for WZM SSE begins at 2.20 V, 0.15 V ahead of $ZnSO_4$ electrolyte, which is probably caused by the catalytic activity of MOF host for water splitting [17]. To verify this, hybrid $ZnSO_4$@MOF-808 (HZM) electrolyte was prepared by impregnating the activated MOF-808 with 1 M $ZnSO_4$ electrolyte (40 wt%). As expected, the OER potential of HZM electrolyte is 2.15 V, which is 0.2 V lower than that of pristine $ZnSO_4$ electrolyte, confirming the influence of MOF host. The MOF itself is electrochemically stable as proved in our previous work about the MOFs with similar SBU for Li SSE [18,19]. It deserves to be noted that an EW of 2.20 V is applicable to all the Zn battery cathodes reported, such as prussian blue analogues [20], MnO_2 [21], VS_2 [22], $Na_3V_2(PO_4)_3$ [23] and V_2O_5 [3], etc. Single-ion conductors possess many advantages over liquid electrolytes. Without any anion movement or accumulation, the attendant concentration polarization can be eliminated [24,25]. Moreover, the inert bulk anionic host can also avoid undesirable side reactions between anions and electrodes during cycling to improve battery performances [26]. Zn^{2+} transference number ($t_{Zn}{}^{2+}$) of WZM SSE was calculated using a Zn|WZM|Zn symmetric cell by Evans method [27] with a constant polarization potential of 10 mV at room temperature. The EIS spectra before and after polarization along with the I-t curve are shown in Fig. 2d. The charge transfer resistance (R_{ct}) increased from about 1260–1340 Ω with decreasing from 4.34 to 4.07 μA for current and thus $t_{Zn}{}^{2+}$ was calculated to be 0.93 accordingly. The $t_{Zn}{}^{2+}$ of WZM SSE is slightly smaller than 1, which is speculated to be caused by the irremovable protons in MOF host as judged by its experimental composition.

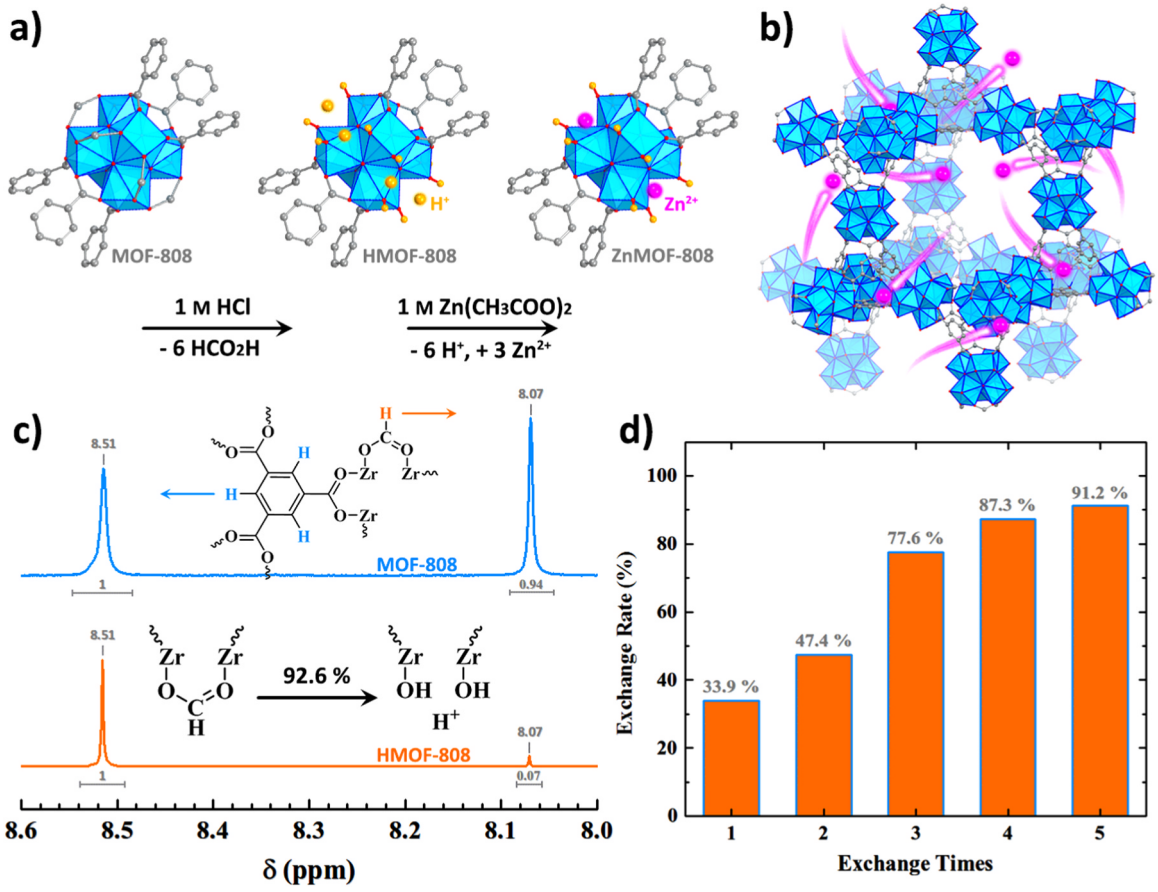

Fig. 1. a) Scheme for the post-synthetic modification chemistry. b) Crystal structure of ZnMOF-808. Blue polyhedrons represent Zr-O clusters and Zn^{2+} ions are highlighted by pink balls. c) ^{1}H NMR of MOF-808 and ZnMOF-808 digested by DCl/DMSO-D_6 (0.1/0.6 mL, DMSO = dimethyl sulfoxide). d) Total Zn^{2+} exchange rates in ZnMOF-808 after different exchange times.

2.3. Uniform and compact Zn deposition

To design solid-state batteries, the solid-solid interfacial contact between SSE and metal anode is required to be stable during cycling. The compatibility of the crystalline single-ion WZM SSE with Zn metal anode was characterized by the galvanostatic Zn plating/stripping performance of a Zn|WZM|Zn symmetric cell. As shown in Fig. 3a, the cycling could be stabilized at a current density of 0.1 mA cm^{-2} over 360 h, during which the voltage profiles were smooth in each cycle and the potential only increased slightly from 0.10 to 0.12 V. Polarization in the first cycle is relatively larger which is caused by the loose contact between SSE and Zn before cycling. Such interfacial contact can be improved through repeated Zn plating/stripping process as proved by the decreased interfacial resistance after cycling (Fig. S8). The Zn foil after cycling was studied by SEM, and a dendrite-free and compact Zn deposition morphology was observed as shown in Fig. 3e, which should be responsible for the stable plating/stripping performance. Zn foil after cycling demonstrates identical XRD (Fig. 3c) with its pristine form, and no ZnO impure phase produced by $Zn(OH)_2$ deposition [2] is recognized. In sharp contrast, as shown in Fig. 3d, many microsized Zn slices with sharp edges appear on the Zn foil after cycling in $ZnSO_4$ electrolyte under the same condition, and the deposition layer is porous and loose, thus bringing the risks of Zn anode pulverization and battery short circuit. Meanwhile, insulated zinc hydrogen sulfate ($Zn(HSO_4)_2$, JCPDS #520258) and ZnO (JCPDS #211486) phases also formed on the Zn foil after cycling according to the XRD result. It worth to be noted that the porous and loose deposition cannot be improved by increasing the Zn^{2+} concentration as indicated by the SEM of the Zn anode after cycling in statured $ZnSO_4$ electrolyte (Fig. S9). It follows that, the WZM SSE possesses much superior compatibility with Zn anode to the conventional liquid electrolytes and the loose and dendritic Zn deposition can be effectively avoided.

The significantly different Zn deposition behavior of WZM SSE from conventional liquid electrolytes was further investigated by monitoring Zn deposition process on the Cu working electrodes. As shown by SEM images in Fig. S10, after 1 h of deposition in $ZnSO_4$ electrolyte, island-like Zn aggregations which were composed by irregularly shaped Zn particles formed on the Cu substrate. These particles further grew into Zn slices and bulk Zn plates with sustaining deposition for 10 h (Fig. S10 right column and Fig. S12a). It should be noted that the Zn deposition in $ZnSO_4$ electrolyte is quite non-uniform with very rough surface, and many areas on Cu foil are still blank as illustrated by the laser scanning confocal microscope (LSCM) optical images with corresponding roughness analysis. For WZM SSE shown in Fig. S11, instead of island-like aggregations, massive nanosized Zn particles can be seen homogenously distributed on the Cu substrate after 1 h deposition. With the deposition continuing, the growth of these particles is uniform forming a compact and smooth Zn deposition layer (Fig. S11 right column and Fig. S12b), which confirms the uniform deposition ability of WZM SSE. Deposition morphologies at higher current were also examined. As shown in Fig. S13, under the same deposition amount (1 mAh cm^{-2}), the size of the deposited particles grows slightly with increasing current density, and the deposition layers remain compact and smooth.

The particular deposition behavior of WZM SSE from liquid electrolyte can be explained by the mechanism shown in Fig. 3b. Apparently, the electrochemical deposition of Zn in $ZnSO_4$ electrolyte follows a classic tip-growth mechanism [28,29]. Initially, Zn metal seeds occur randomly on the Cu substrate at the beginning of deposition due to various fluctuations in the system. As we all know, a sharp edge or protrusion on the electrode indicates a stronger electrical field, so more

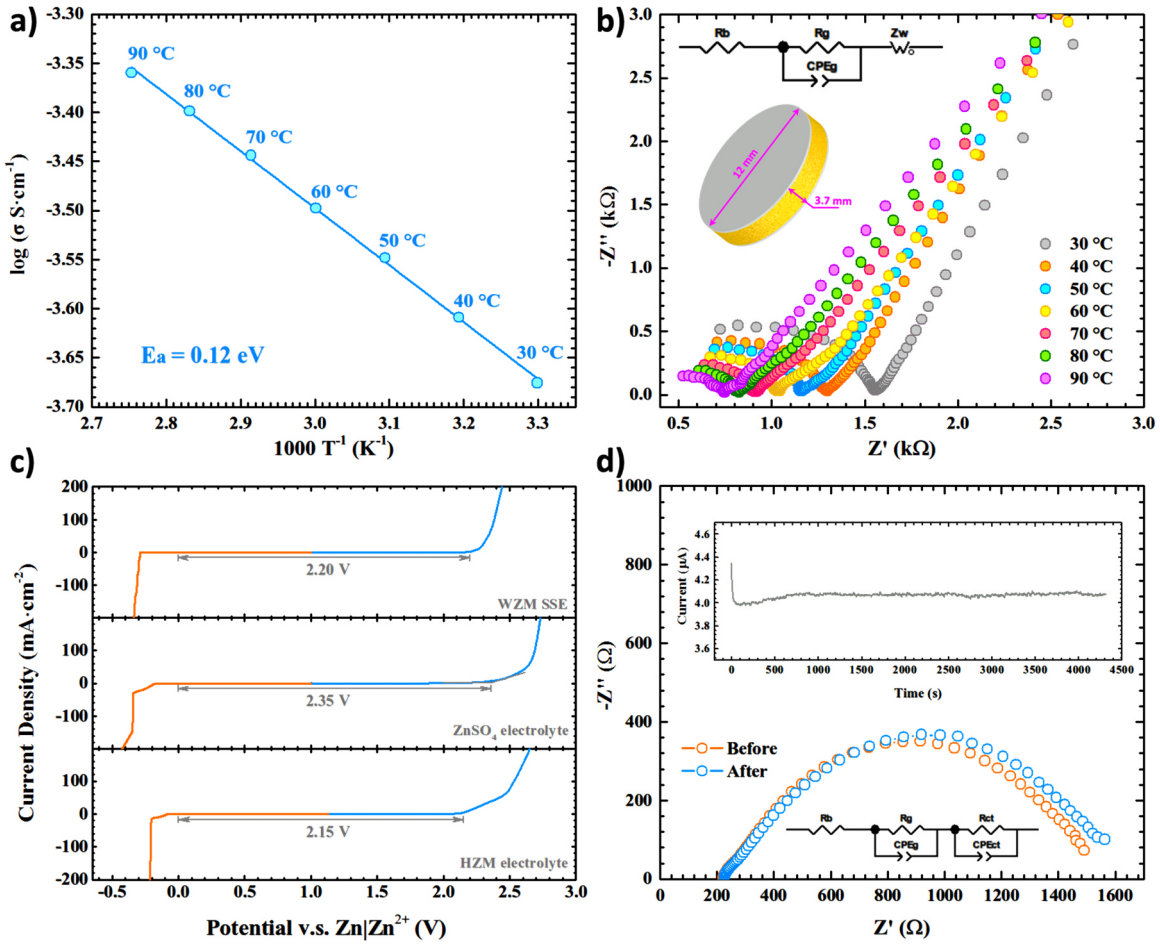

Fig. 2. a) Arrhenius plot for the ionic conductivities and b) corresponding EIS curves with equivalent circuit of WZM SSE from 30° to 90 °C, inset: size of the SSE pellet for EIS test. c) Electrochemical windows of WZM SSE, $ZnSO_4$ electrolyte and HZM electrolyte at room temperature. d) EIS of the Zn|WZM|Zn symmetric cell before and after polarization and corresponding equivalent circuit, inset: variation of current with time during polarization at an applied voltage of 10 mV at room temperature.

Zn will be preferentially deposited around the tips rather than on blank regions of the Cu substrate. In $ZnSO_4$ aqueous electrolyte (left column of Fig. 3b), such growth is uncontrollable because the depleted Zn^{2+} ions around the tips will be rapidly replenished owing to their fast long-range movability in bulk liquid phase, and thus Zn growth on the blank regions of Cu substrate is highly suppressed. The vertical free tip-growth of Zn in $ZnSO_4$ electrolyte eventually results in bulk aggregations and non-uniform deposition. Conversely, the transport of the Zn $(H_2O)_6^{2+}$ ions in WZM SSE (middle column of Fig. 3b) is guided by the subnano-tunnels in MOF host, and Zn deposition happens at a restricted nanowetted interface between WZM SSE and Zn metal, which is created by H_2O release from desolvation of the confined $Zn(H_2O)_6^{2+}$ that causing interfacial wetting and Zn^{2+} deposition. Therefore, large Zn plate aggregations caused by free tip-growth are avoided through the guided and restricted Zn plating in WZM SSE, resulting in uniform Zn plating rate over the entire Zn anode surface.

To justify the proposed deposition mechanism of WZM SSE, the deposition morphologies in HZM electrolyte were also studied. As shown in Fig. S14, the deposited Zn is also homogeneously covered on Cu substrate without bulk plates/protrusions, but its microstructure, which demonstrates a mossy layer of porous Zn slices, is identical with those observed in pristine $ZnSO_4$ electrolyte. Thus, it can be concluded that the uniform Zn deposition is indeed resulted from the solid microporous MOF host with nanowetted interface, while the deposited microstructure has a different origin. The difference between WZM SSE and HZM for Zn metal deposition can be attributed to the fact that the anionic MOF host is fixed and only the Zn $(H_2O)_6^{2+}$ cations are movable under electrochemical driving force in WZM SSE, which leads to the guided and restricted Zn plating along the nanowetted Zn/SSE interface and results in the homogeneous and compact microstructure. In contrast, both anions (solvated SO_4^{2-}) and cations (Zn $(H_2O)_6^{2+}$) in MOF-808 are movable for HZM (right column of Fig. 3b). They can transfer together through the nanowetted interface between HZM and Zn metal and deposit at different regions of Zn metal surface with various deposition rates, which leads to the growth of porous Zn slices (i.e. free tip-growth in micro-scale). Taken together, these results and analyses suggest that such homogeneous, compact and smooth Zn deposition should be uniquely featured by the single-ion Zn^{2+} SSE.

2.4. Rechargeable VS_2/Zn batteries with WZM SSE

To further demonstrate the performance of WZM SSE, VS_2/Zn solid-state batteries (SSBs) were assembled and tested. Cathode material of layered VS_2 was prepared according to the reported procedures [22], and its purity and morphology were characterized by XRD and SEM, as shown in Fig. S15. Free-standing cathodes were prepared by rolling a jelly mixture of VS_2, acetylene black, and poly(1,1,2,2-tetrafluoroethylene) (PTFE) binder. WZM SSE was directly pressed on the cathode forming a double-layered structure (Fig. S16), which was then assembled into coin cell with Zn metal as anode. The WZM SSE layer shows a high Yong's modulus of 5.3 GPa and micro-indentation hardness of 0.22 GPa, ensuring good mechanical stability of the solid battery. Cycling performance of the Zn SSB at room temperature is shown in Fig. 4a. It demonstrates a reversible capacity of 125 mAh g^{-1} (89% of the initial

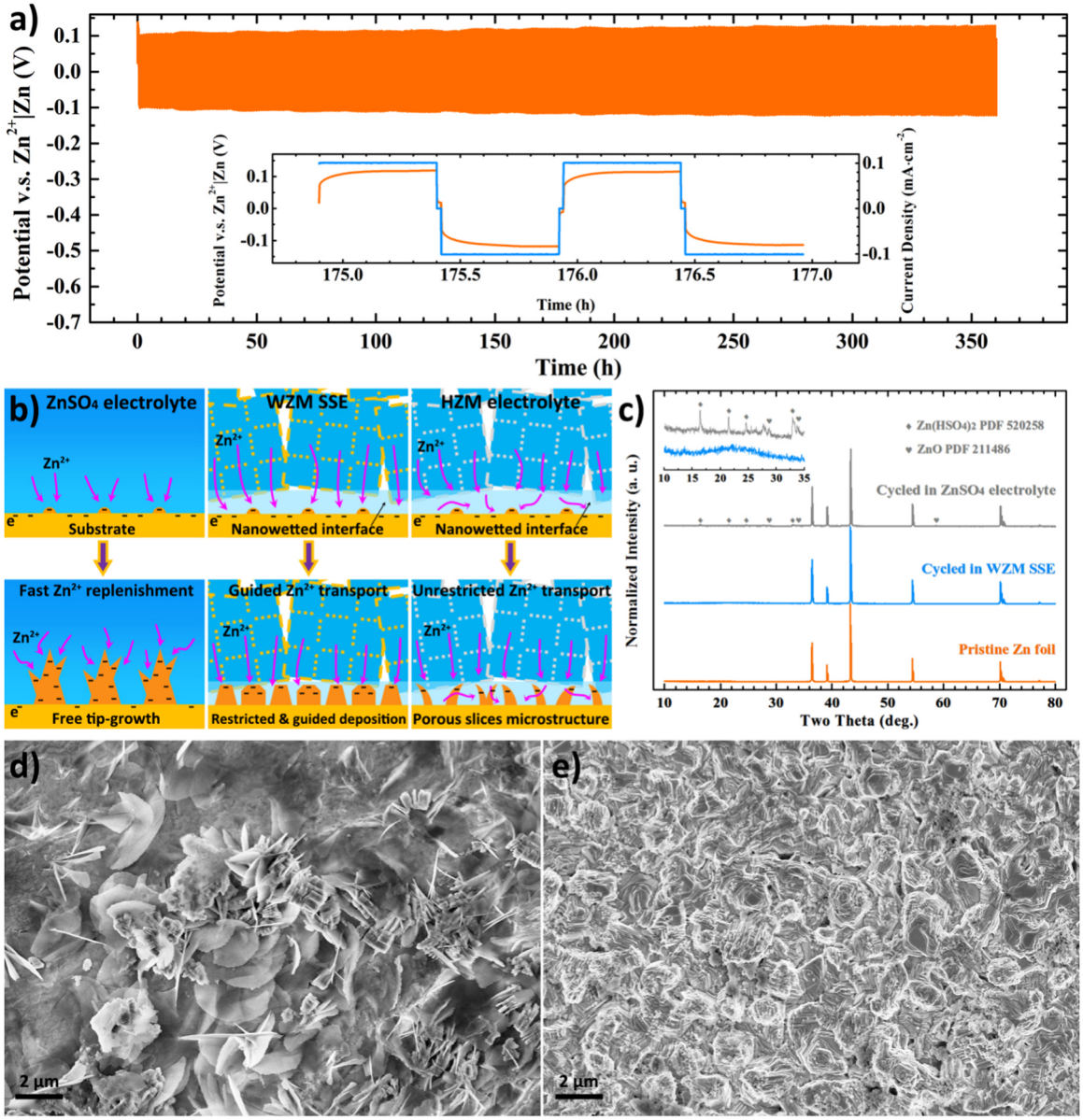

Fig. 3. a) Zn plating/stripping performance of the Zn|WZM|Zn symmetric cell under a current density of 0.1 mAcm^{-2} at room temperature. b) Proposed mechanism for the different deposition behaviours of $ZnSO_4$ aqueous electrolyte (left column), WZM SSE (middle column) and HZM electrolyte (right column). c) XRD patterns of the Zn foils before (orange) and after plating/stripping cycles in WZM SSE (blue) and $ZnSO_4$ electrolyte (grey), respectively. SEM images of the Zn foils after plating/stripping cycles of d) Zn|$ZnSO_4$|Zn cell and e) Zn|WZM|Zn cell.

cycle) at 0.2 A g^{-1} charge/discharge rate with a high Coulombic efficiency of 99.7% after 250 cycles. The high Coulombic efficiency indicates that the parasitic H_2 and O_2 evolutions which often happen in aqueous batteries are negligible during cycling, promising a long battery life. Rate capability and corresponding charge/discharge curves at different current rate are shown in Figs. 4b and 4c. Two distinguished discharge plateaus can be observed corresponding to a two-step Zn intercalation, i.e. $VS_2 \rightarrow Zn_{0.09}VS_2$ and $Zn_{0.09}VS_2 \rightarrow Zn_{0.23}VS_2$, respectively [22]. About 40% capacity retention at 2 A g^{-1} is obtained compared to 0.1 A g^{-1}, and the capacity recoverability is good when the current goes back to 0.1 A g^{-1}. As a comparison, rate capability of VS_2/Zn battery in liquid $ZnSO_4$ electrolyte was also tested, as shown in Fig. S17. Although the polarization of the solid cell is larger at high current rate, it possesses equal capacities with its counterpart at low current rate. By resting the fully charged cell for 24 h, 97.5% of the original capacity was retained, which confirms an acceptable self-discharge rate of the Zn SSB. The good performances of such prototype Zn SSBs reflects that the crystalline single-ion Zn^{2+} SSE is practicable and reliable in actual devices.

3. Conclusions

In conclusion, the first crystalline single-ion Zn^{2+} solid-state electrolyte (WZM SSE) is designed based on the post-synthetic modified MOF-808. By virtue of the highly concentrated $Zn(H_2O)_6^{2+}$ ions contained in the pores of MOF host, it demonstrates a high conductivity of 2.1×10^{-4} S cm^{-1} at 30 °C with small activation energy of 0.12 eV. The single-ion conducting behavior of WZM SSE is confirmed by its high Zn^{2+} transference number of 0.93. The porous structure of the MOF host can be retained under a high compressing force, proving its sufficient mechanical strength for battery applications. Electrochemical window of WZM SSE is above 2.2 V, which is applicable to all the Zn battery cathodes reported before. Compared with $ZnSO_4$ aqueous electrolyte, WZM SSE shows superior compatibility with Zn metal anode. The homogeneous Zn plating over the entire Zn anode surface is attributed to the guided and restricted Zn deposition through the nanowetted Zn/SSE interface, while the compact and smooth deposited microstructure origins from the confined $Zn(H_2O)_6^{2+}$ ions within the fixed

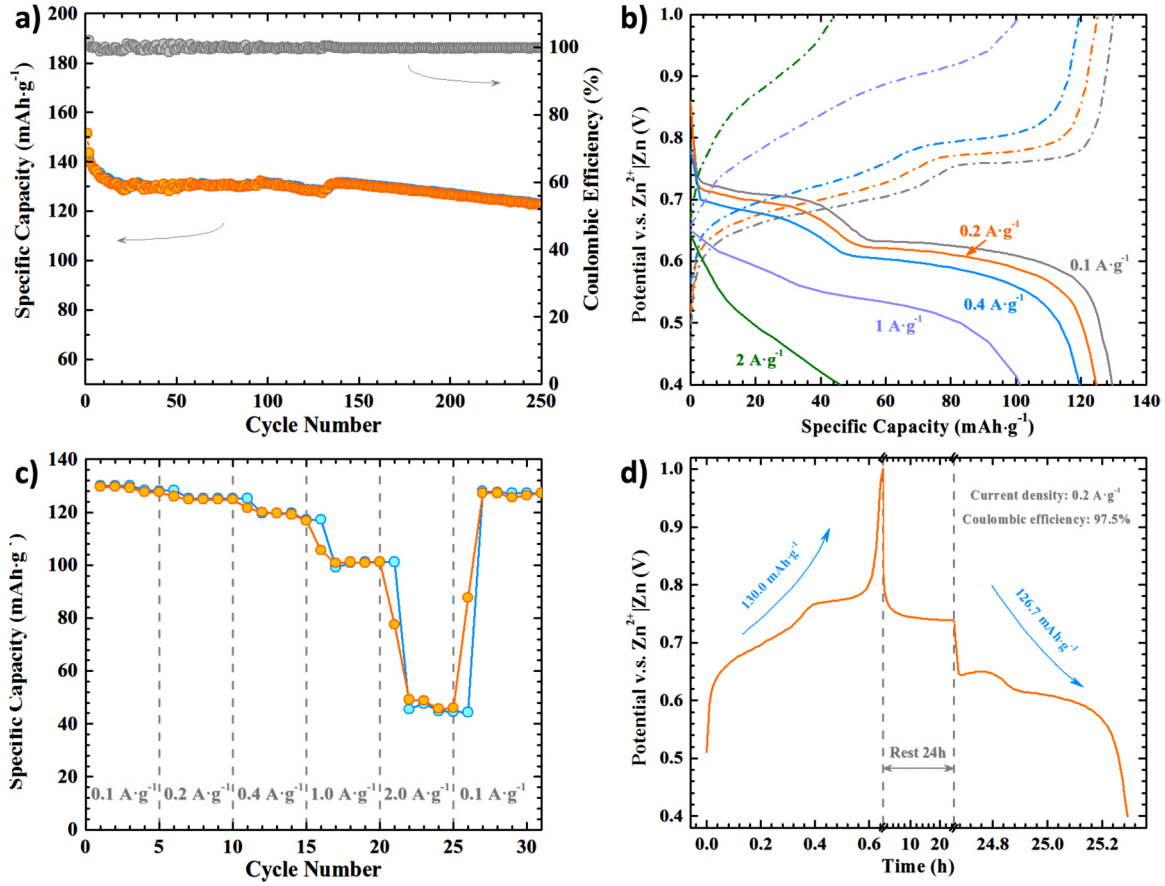

Fig. 4. Battery performances of the VS_2/Zn solid battery at room temperature. a) Cycle performance at 0.2 A g^{-1}. b) Charge/discharge profiles and c) capacities after being activated for 20 cycles at different current rates. d) Self-discharge test by resting for 24 h at fully charged state after 20 cycles at 0.2 A g^{-1}.

anionic MOF host. Inspired by all these advantages, WZM SSE is further investigated in the actual VS_2/Zn batteries which demonstrate both good cyclability and rate capability with very small self-discharge rates. In the end, by tuning the species of cations and solvent guests in MOFs, more special single-ion SSEs that are currently non-existent would be further acquired, thus providing great opportunities for the development of novel solid-state electrochemistry.

4. Experimental section

4.1. Materials

MOF-808: $[Zr_6O_4(OH)_4(HCOO)_6(C_9H_3O_6)_2]$. 3.4 g $ZrOCl_2{\cdot}8H_2O$, BTC, 200 mL N,N-dimethylformamide (DMF), and 200 mL formic acid were sequentially added into a 500 mL glass jar and stirred for 30 min at room temperature. Then the glass jar was sealed and heated at 100 °C for 48 h. After cooling down, MOF-808 nano-crystals were collected by centrifuging and washed with DMF and acetone, which were activated at 150 °C in vacuum before use.

HMOF-808: $[Zr_6O_4(OH)_4(OH)_{12}H_6(C_9H_3O_6)_2]$ (cal.), $[Zr_6O_4(OH)_4(OH)_{11.16}H_{5.58}(HCOO)_{0.42}(C_9H_3O_6)_2]$ (exp.). 4 g MOF-808 and 400 mL 1 M HCl were loaded into a 500 mL flask and heated at 90 °C for 24 h with continuous stirring. After cooling down, HMOF-808 was collected by centrifuging and washed with water until the supernatant became neutral. About 92.6% of the SBUs were converted based on the -HCOO- group as indicated by the ^{1}H NMR results, and the experimental composition of HMOF-808 was determined accordingly.

ZnMOF-808: $[Zr_6O_4(OH)_4(OH)_{12}Zn_3(C_9H_3O_6)_2]$ (cal.), $[Zr_6O_4(OH)_4(OH)_{11.16}H_{0.18}Zn_{2.7}(HCOO)_{0.42}(C_9H_3O_6)_2]$ (exp.). For cation exchange, 0.5 g HMOF-808 was dispersed in 7 mL 1 M zinc acetate solution, which was stirred for 24 h at room temperature. The cation exchange process was repeated 4 times to achieve an exchange rate of 91.2% based on the ICP results of Zn^{2+}/Zr^{4+} ratio. After cation exchange, the ZnMOF-808 was washed with water and activated at 150 °C in vacuum for 12 h.

WZM SSE: WZM SSE was obtained by filling the pores of ZnMOF-808 with H_2O molecule guests to generate cationic $Zn(H_2O)_6^{2+}$ and anionic MOF host. Typically, about 30 wt% H_2O could be absorbed by the activated ZnMOF-808 after being treated at 60 °C, 90% RH for 24 h, as indicated by the TGA results, and the Zn^{2+} content of WZM SSE is calculated to be 8.3 wt%.

VS_2 Flake: The VS_2 cathode material was prepared following the routes reported elsewhere [22]. 0.351 g NH_4VO_3 was dissolved by 45 mL H_2O and 3 mL ammonia and then 1.7 g thioacetamide was added in the solution. The mixture was stirred for 1 h at room temperature which was transferred into a 100 mL autoclave and heated at 180 °C for 12 h. VS_2 flake was collected by filtering, washed with water and ethanol and dried at 60 °C in vacuum.

Battery Assembly: WZM SSE was pressed into a 12 mm pellet (about 3.7 mm thick) under 10 t force, sandwiched between two SS electrodes and sealed with resin to conduct the EIS tests form 30–90 °C. Similarly, thinner pellets (about 0.3 mm thick) were also prepared using 50 mg WZM SSE (containing 5 wt% PTFE binder to increase the toughness and strength of the pellet) and were fabricated into CR2032 cells for LSV and Zn plating/stripping tests. For VS_2/Zn solid battery assembly, VS_2, acetylene black and PTFE (60 wt% emulsion) were dispersed in isopropanol in a weight ratio of 7: 2: 1. The mixture was milled and rolled into a free-standing membrane, which was cut into ϕ 7 mm round pieces and dried at 80 °C in vacuum as the cathodes. The VS_2 cathodes (about 2 mg cm^{-2}) were immersed in 1 M $ZnSO_4$ aqueous electrolyte over night before use. For Zn battery assembly, 50 mg WZM SSE (containing 5 wt% PTFE binder) was pressed onto the VS_2

cathode in a ϕ 12 mm die under 10 t force. CR2032 coin cells were assembled and tested using the double-layered pellet as cathode and SSE, and Zn foil as anode.

4.2. Characterizations

XRD patterns of MOF-808, HMOF-808 and ZnMOF-808 powders and ZnMOF-808 pellets were recorded by a Bruker D8 Advance diffractometer using Cu Kα, λ = 1.541 Å. SEM images of these MOF materials and Zn deposition morphologies were taken with a Zeiss Supra 55 scanning electron microscope. LSCM images and roughness analysis of Zn deposition morphologies were acquired with a Keyence VK-X200 microscope. N_2 adsorption-desorption isothermals of MOF-808 and ZnMOF-808 were recorded on a Micromeritics ASAP 2020 HD88 tool. TGA tests of MOF-808, ZnMOF-808 and WZM SSE were carried out on a N_2 atmosphere at a scan speed of 10 °C min^{-1} on a Mettler Toledo TGA/DSC Star system. ^{1}H NMR tests of the digested MOF (DCl/DMSO-D_6, 0.1/0.6 mL) were performed on a Bruker Avance-III 400 Plus system. ICP of ZnMOF-808 digested by 40 wt% H_2SO_4 solution was tested on a Horiba JY 2000 instrument. Young's modulus and indentation hardness of the SSE pellet were tested with an Agilent G200 nano indenter. EIS, LSV and Zn plating/stripping measurements were performed on a Solartron Analytical electrochemical workstation. The cycling performance of VS_2/Zn batteries with WZM SSE and $ZnSO_4$ electrolyte were tested by LAND CT2001A battery test system.

Acknowledgements

This work was financially supported by National Key R&D Program of China (2016YFB0700600), the National Natural Science Foundation of China (51672012), Shenzhen Science and Technology Research Grant (JCYJ20150729111733470, JCYJ20151015162256516), and China Postdoctoral Science Foundation (2017M620520).

Appendix A. Supporting information

Supplementary data associated with this article can be found in the online version at doi:10.1016/j.nanoen.2018.11.038.

References

[1] D. Kundu, B.D. Adams, V. Duffort, S.H. Vajargah, L.F. Nazar, Nat. Energy 1 (2016) 16119.
[2] F. Wang, O. Borodin, T. Gao, X. Fan, W. Sun, F. Han, A. Faraone, J.A. Dura, K. Xu, C. Wang, Nat. Mater. 17 (2018) 543–549.
[3] J. Zhou, L. Shan, Z. Wu, X. Guo, G. Fang, S. Liang, Chem. Commun. 54 (2018) 4457–4460.
[4] H. Pan, Y. Shao, P. Yan, Y. Cheng, K.S. Han, Z. Nie, C. Wang, J. Yang, X. Li, P. Bhattacharya, K.T. Mueller, J. Liu, Nat. Energy 1 (2016) 16039.
[5] C. Xu, B. Li, H. Du, F. Kang, Angew. Chem. Int. Ed. 51 (2012) 933–935.
[6] K. Litao, C. Mangwei, J. Fuyi, G. Yanfeng, L. Hongjie, L. Jianjun, L. Wei, Z. Chunyi, Adv. Energy Mater. 8 (2018) 1801090.
[7] N. Zhang, F. Cheng, Y. Liu, Q. Zhao, K. Lei, C. Chen, X. Liu, J. Chen, J. Am. Chem. Soc. 138 (2016) 12894–12901.
[8] R. Chen, W. Qu, X. Guo, L. Li, F. Wu, Mater. Horiz. 3 (2016) 487–516.
[9] C. Yang, K. Fu, Y. Zhang, E. Hitz, L. Hu, Adv. Mater. 29 (2017) 1701169.
[10] R. Guduru, J. Icaza, Nanomaterials 6 (2016) 41.
[11] S.S. Park, Y. Tulchinsky, M. Dincă, J. Am. Chem. Soc. 139 (2017) 13260–13263.
[12] J. Cepeda, S. Pérez Yáñez, G. Beobide, O. Castillo, E. Goikolea, F. Aguesse, L. Garrido, A. Luque, P.A. Wright, Chem. Mater. 28 (2016) 2519–2528.
[13] Z. Wang, S.M. Cohen, Chem. Soc. Rev. 38 (2009) 1315–1329.
[14] R. Ameloot, M. Aubrey, B.M. Wiers, A.P.G.ómora Figueroa, S.N. Patel, N.P. Balsara, J.R. Long, Chem. Eur. J. 19 (2013) 5533–5536.
[15] H. Furukawa, F. Gándara, Y. Zhang, J. Jiang, W.L. Queen, M.R. Hudson, O.M. Yaghi, J. Am. Chem. Soc. 136 (2014) 4369–4381.
[16] P. Ji, J.B. Solomon, Z. Lin, A. Johnson, R.F. Jordan, W. Lin, J. Am. Chem. Soc. 139 (2017) 11325–11328.
[17] K. Meyer, M. Ranocchiari, J.A. van Bokhoven, Energy Environ. Sci. 8 (2015) 1923–1937.
[18] Z. Wang, R. Tan, H. Wang, L. Yang, J. Hu, H. Chen, F. Pan, Adv. Mater. 30 (2018) 1704436.
[19] Z. Wang, Z. Wang, L. Yang, H. Wang, Y. Song, L. Han, K. Yang, J. Hu, H. Chen, F. Pan, Nano Energy 49 (2018) 580–587.
[20] Z. Liu, G. Pulletikurthi, F. Endres, ACS Appl. Mater. Interfaces 8 (2016) 12158–12164.
[21] B. Wu, G. Zhang, M. Yan, T. Xiong, P. He, L. He, X. Xu, L. Mai, Small 14 (2018) 1703850.
[22] P. He, M. Yan, G. Zhang, R. Sun, L. Chen, Q. An, L. Mai, Adv. Energy Mater. 7 (2017) 1601920.
[23] G. Li, Z. Yang, Y. Jiang, C. Jin, W. Huang, X. Ding, Y. Huang, Nano Energy 25 (2016) 211–217.
[24] J.F. Van Humbeck, M.L. Aubrey, A. Alsbaiee, R. Ameloot, G.W. Coates, W.R. Dichtel, J.R. Long, Chem. Sci. 6 (2015) 5499–5505.
[25] D.R. Sadoway, B. Huang, P.E. Trapa, P.P. Soo, P. Bannerjee, A.M. Mayes, J. Power Sources 97-98 (2001) 621–623.
[26] E. Quartarone, P. Mustarelli, Chem. Soc. Rev. 40 (2011) 2525–2540.
[27] J. Evans, C.A. Vincent, P.G. Bruce, Polymer 28 (1987) 2324–2328.
[28] F. Ding, W. Xu, G.L. Graff, J. Zhang, M.L. Sushko, X. Chen, Y. Shao, M.H. Engelhard, Z. Nie, J. Xiao, X. Liu, P.V. Sushko, J. Liu, J. Zhang, J. Am. Chem. Soc. 135 (2013) 4450–4456.
[29] J.W. Diggle, A.R. Despic, J.O.M. Bockris, J. Electrochem. Soc. 116 (1969) 1503–1514.

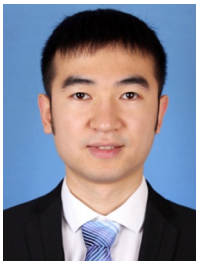

Ziqi Wang received his Ph.D. degree under the supervision of Prof. Guodong Qian at Zhejiang University (China) in 2016. Dr. Wang is currently a postdoctoral researcher at the School of Advanced Materials, Peking University Shenzhen Graduate School (China) in Prof. Feng Pan's group. His research interests focus on metal-organic frameworks (MOFs) and their applications in electrochemical energy storage.

Jiangtao Hu received his B.S. degree from Henan University in 2013, China. Hu is now pursuing his Ph.D. degree under the supervision of Prof. Feng Pan at the School of Advanced Materials, Peking University Shenzhen Graduate School, China. His research interests mainly lie in design and development of functional materials for energy storage and conversion applications such as batteries, supercapacitors, and catalysis.

Han Lei received his B.S. degree in 2016 from Peking University, China. He is pursuing his M.S. degree in the School of Advanced Materials, Peking University Shenzhen Graduate School, China. His research interests include advanced functional materials and their new application in energy storage and conversion devices, such as all solid-state batteries, conductive polymers, and so on.

Zijian Wang received his B.S. degree from the School of Materials Science and Engineering at Nanchang University (China) in 2016. Wang is now pursuing his Ph.D. degree under the supervision of Prof. Feng Pan at the School of Advanced Materials, Peking University Shenzhen Graduate School, China. His research interests focus on developing novel solid-state electrolytes for all-solid-state Li batteries.

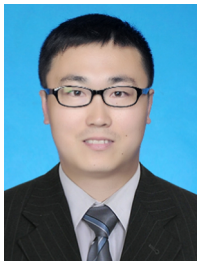

Hongbin Wang received his B.S. degree from the School of Materials Science and Engineering at Jilin University (China) in 2009, and earned Ph.D. degree from the School of Chemistry at Jilin University in 2015 under the supervision of Prof. Zongtao Zhang. Dr. Wang is now pursuing his postdoctoral training with Prof. Feng Pan at the School of Advanced Materials, Peking University Shenzhen Graduate School, China. His research interests mainly lie in exploring key materials and technologies for energy storage and conversion applications including lithium ion batteries, sodium ion batteries, and supercapacitors.

Jiajie Liu is currently a Ph.D. candidate in Prof. Feng Pan's group at Peking University Shenzhen Graduate School, China. He received his B.S. degree in Chemistry from Peking University in 2016. Currently his research interests focus on high energy density cathode materials for Li-/Na-ion batteries, especially on layered oxide materials including Li- and Mn-rich layered oxides and Ni-rich layered oxides.

Qinghe Zhao received his B.S. degree from the School of Materials Science and Engineering at University of Science and Technology of Beijing (USTB, China) in 2010, and earned Ph.D. degree from the School of Advanced Materials at USTB in 2016, majoring in the electrochemical corrosion behavior of iron-based alloys, under the supervision of Prof. Minxu Lu. Dr. Zhao is now accepting his postdoctoral training with Prof. Feng Pan at the School of Advanced Materials, Peking University Shenzhen Graduate School, China. His research interests mainly focus on the key materials and technologies for energy storage and conversion applications, including electrocatalysts, zinc ion batteries, and sodium ion batteries.

Feng Pan, founding Dean of School of Advanced Materials, Peking University Shenzhen Graduate School, got B.S. from Dept. Chemistry, Peking University in 1985 and Ph.D. from Dept. of P&A Chemistry , University of Strathclyde, Glasgow, UK, with “Patrick D. Ritchie Prize” for the best Ph.D. in 1994. With more than a decade experience in large international incorporations, Prof. Pan has been engaged in fundamental research and product development of novel optoelectronic and energy storage materials and devices. As Chief Scientist, Prof. Pan led eight entities in Shenzhen to win 150 million RMB grant for the national new energy vehicles (power battery) innovation project since 2013.